Comparison of the structural and chemical composition of two unique micro/nanostructures produced by femtosecond laser interactions on nickel

Craig A. Zuhlke, Troy P. Anderson, and Dennis R. Alexander

Citation: Applied Physics Letters **103**, 121603 (2013); doi: 10.1063/1.4821452
View online: http://dx.doi.org/10.1063/1.4821452
View Table of Contents: http://scitation.aip.org/content/aip/journal/apl/103/12?ver=pdfcov
Published by the AIP Publishing

Articles you may be interested in

Ultrashort laser pulse induced nanogratings in borosilicate glass
Appl. Phys. Lett. **104**, 211107 (2014); 10.1063/1.4880658

Grain boundary diffusivity of Ni in Au thin films and the associated degradation in electrical contact resistance due to surface oxide film formation
J. Appl. Phys. **113**, 114906 (2013); 10.1063/1.4795768

The influence of laser-induced nanosecond rise-time stress waves on the microstructure and surface chemical activity of single crystal Cu nanopillars
J. Appl. Phys. **113**, 084309 (2013); 10.1063/1.4793646

High-aspect-ratio grooves fabricated in silicon by a single pass of femtosecond laser pulses
J. Appl. Phys. **111**, 093102 (2012); 10.1063/1.4709726

Magnetic and morphological characteristics of nickel nanoparticles films produced by femtosecond laser ablation
Appl. Phys. Lett. **85**, 4103 (2004); 10.1063/1.1815065

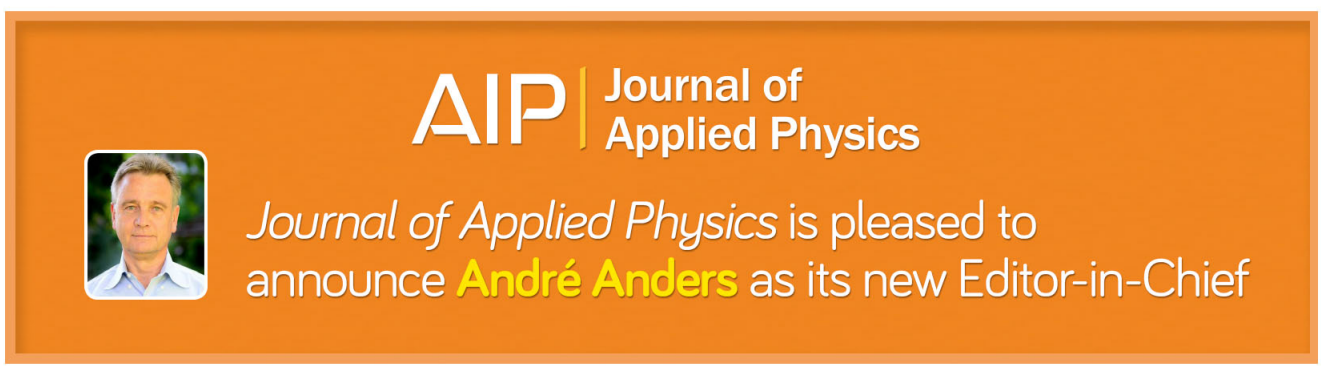

This article is copyrighted as indicated in the article. Reuse of AIP content is subject to the terms at: http://scitation.aip.org/termsconditions. Downloaded to IP: 129.93.64.70 On: Fri, 22 Aug 2014 16:36:15

Comparison of the structural and chemical composition of two unique micro/nanostructures produced by femtosecond laser interactions on nickel

Craig A. Zuhlke,[a] Troy P. Anderson, and Dennis R. Alexander
Department of Electrical Engineering, University of Nebraska-Lincoln, Lincoln, Nebraska 68588, USA

(Received 19 June 2013; accepted 2 September 2013; published online 18 September 2013)

The structural and chemical composition of two unique microstructures formed on nickel, with nanoscale features, produced using femtosecond laser surface processing (FLSP) techniques is reported in this paper. These two surface morphologies, termed mounds and nanoparticle-covered pyramids, are part of a larger class of self-organized micro/nanostructured surfaces formed using FLSP. Cross-sections of the structures produced using focused ion beam milling techniques were analyzed with a transmission electron microscope. Both morphologies have a solid core with a layer of nanoparticles on the surface. Energy dispersive X-ray spectroscopy by scanning transmission electron microscopy studies reveal that the nanoparticles are a nickel oxide, while the core material is pure nickel. © *2013 AIP Publishing LLC*. [http://dx.doi.org/10.1063/1.4821452]

Femtosecond laser surface processing (FLSP) is rapidly emerging as a powerful and flexible technique for the fabrication of functionalized multiscale surfaces. By simultaneously modifying both surface morphology and surface chemistry, FLSP can be utilized to modify the physical, chemical, mechanical, and electrical properties of a target material without the deposition of additional materials. FLSP is utilized to generate wide-band optical absorbers such as black silicon,[1–4] colored metals,[5] and biologically inspired surfaces with tailored wettability.[6–9] However, the application of FLSP for the fabrication of advanced materials is still in the early stages. Much of the current understanding of the different surface morphologies that can be created on a given material via FLSP has been derived from phenomenological studies based on the empirical demonstration of a laser-processed surface structure. There is a critical need to better understand the laser-material interactions that lead to the development of multiscale surfaces in order to tailor the size, shape, and structural properties of a surface for a given application. Additionally, previous studies have demonstrated that various laser and environmental parameters can be used to influence the induced surface morphology. For example, the size of micro-structures is a function of the laser fluence,[10,11] the structure protrusion angle is a function of the angle of incidence of the laser beam,[12] the eccentricity of the structures can be tuned through laser polarization,[12–14] and the shape of the micro-structures can be controlled via the atmosphere during irradiation.[3,10,15–17] However, the very parameters used to control the shape and size also control the growth mechanisms and thus the structural and chemical composition of the structures themselves. Therefore, these processing parameters cannot be indiscriminately altered to tailor the overall surface morphology without regard to structural effects. We have recently demonstrated, for example, that the laser fluence critically influences not only the geometry of the surface structures but also the fundamental mechanisms that are responsible for the formation of the structures.[18] In the present work, we expand on the previous study and demonstrate that the mechanisms through which surface structures develop also critically affects the final structural and crystalline composition of the processed surface.

In this work, the impact of the growth mechanism of multiscale surface structures fabricated via FLSP is characterized through an analysis of surface structures fabricated with a laser fluence ~40 times above the ablation threshold (named mounds) and surface structures fabricated with a laser fluence ~3 times above the ablation threshold (named nanoparticle-covered pyramids (NC-pyramids)). The ablation threshold for nickel is 0.05 J/cm^2 when measured with 300 fs pulses centered at 527 nm.[19] The surfaces fabricated with the larger laser fluence are similar to previously published mound structures,[18] and the structures fabricated with the lower laser fluence are similar to the previously published NC-pyramid structures.[20,21]

Our previous publications include full descriptions of the formation process for the both mounds[18,20] and NC-pyramids.[20,21] A brief overview of the formation processes is included here to help clarify the structural and chemical analysis results. In our previous publication, the mound structures were separated into two unique morphologies: above surface growth mounds (ASG-mounds) and below surface growth mounds (BSG-mounds).[18] The fluence of the ablation pulses determines which morphology develops, with the ASG-mounds forming at a higher fluence than the BSG-mounds. ASG-mounds form over ~100 pulses and BSG-mounds from over ~1000 pulses. The formation of both categories of mounds begins with the development of precursor domes that serve to initiate the later formation processes. Once the precursor domes are established, ASG-mound formation is dominated by fluid flow of the surface melt induced by non-uniform heating of the surface, along with redeposition of ablated material. Both of these mechanisms result in upward growth of the structures building on top of the precursor domes. The late stages of BSG-mound formation are dominated by preferential ablation of the

[a]Author to whom correspondence should be addressed. Electronic mail: czuhlke11@gmail.com.

 © 2013 AIP Publishing LLC

This article is copyrighted as indicated in the article. Reuse of AIP content is subject to the terms at: http://scitation.aip.org/termsconditions. Downloaded to IP: 129.93.64.70 On: Fri, 22 Aug 2014 16:36:15

valleys between each BSG-mound initialized by the precursor domes. This growth mechanism results in structures with peaks that are always below the original surface.

NC-pyramid formation is a different type of process than the formation of either mound structures and begins with the development of precursor cones. The precursor cones form due to localized increases in the ablation threshold of the surface, leading to preferential ablation of the material around the contrasting cone site. The cones have the same aspect ratio and slope of the final structure and develop from preferential ablation around locations of increased ablation threshold. Once a cone is established, the structure continues to develop into the sample surface through preferential ablation of the flat regions between individual NC-pyramids. At the same time, nanoparticles created during the ablation process redeposit on the surface. As a result, the structure grows taller and larger in diameter with increased pulse count, but the growth layer is composed of nanoparticles and is therefore porous.[20,21]

Mounds and NC-pyramids were fabricated on nickel by translating the target sample through the path of femtosecond laser pulses in a raster pattern. The laser used for the fabrication of multiscale surface structures was a Spectra Physics Spitfire, Ti:Sapphire femtosecond laser system. The system is capable of producing 1 mJ, 50 fs pulses with a 1 kHz repetition rate. The pulse length and chirp were monitored using a Frequency Resolved Optical Gating (FROG) instrument from Positive Light (Model 8-02). The position of the sample with respect to the laser focal volume was controlled using computer-guided Melles Griot nanomotion translation stages with 3 axes of motion. The laser power was controlled using a half-wave plate and a polarizer.

Previous studies have demonstrated that the growth of self-organized surface structures is critically dependent on the laser fluence. For this reason, a square-shaped flat-top beam profile was used for the experiments in order to generate an uniform laser fluence on the material surface. This beam profile was created using a refractive beam shaper from Eksma Optics (GTH-4-2.2FA). The experimental setup including a more detailed description of the flat-top profile and a description of the determination of the spot size can be found in our previous publication.[18] Processed regions larger than the laser spot size were created by translating the sample through the laser path in a raster pattern; the number of pulses incident on the sample was controlled via the translation speed. The work presented here was completed using nickel (200/201), which was chosen because of its promising use as electrodes in pseudocapacitor and electrolysis systems, its purity, and the amount of published work on femtosecond pulse interactions with nickel.

The mounds discussed in the current work were produced at a laser fluence of 1.99 J/cm^2, which is in the crossover region between ASG-mounds and BSG-mounds; the formation process is therefore expected to be a combination of preferential ablation, fluid flow of the surface melt, and redeposition of material/nanoparticles. The size of the square top-hat beam profile was 168 μm per side and the translation speed and pitch between raster passes of the sample during fabrication was 2 mm/s and 15 μm, respectively, which resulted in 940 pulses per area. The NC-pyramids were formed with a laser fluence of 0.15 J/cm^2. The size of the beam profile was 290 μm per side, the translation speed of the sample was 0.5 mm/s, and the pitch between raster passes was 10 μm, which corresponds to 16 820 pulses per area. All samples were produced from the same stock of nickel, in open air and at a temperature of 22 °C.

A single mound and NC-pyramid from the laser processed samples were investigated using a transmission electron microscope (TEM) and energy-dispersive X-ray spectroscopy (EDX) analysis. Cross-sections of representative mound and NC-pyramid structures were obtained via the *in situ* focused ion beam (FIB) lift out technique using a FEI Strata Dual Beam FIB/SEM. Each sample was capped with a carbon layer prior to the FIB milling to protect the nanoparticles on the surface from the high energy ion beam. TEM analysis was then performed using a FEI Tecnai TF-20 FEG/TEM. Images were taken at 200 kV in bright-field (BF) TEM mode and high-angle annular dark-field (HAADF) scanning transmission electron microscopy (STEM) mode. To obtain chemical analysis, EDX spectra were obtained in STEM mode using a nominal 2 nm electron beam and an EDX detector system produced by EDAX.

Since this work focuses on chemical analysis of structures formed through FLSP, great care was taken to ensure the samples were not contaminated during the perpetration process. Our past experience has shown that any imaging in a scanning electron microscope (SEM) can often lead to surface contaminations of samples with hydrocarbons which originates from the SEM vacuum pumps. With this in mind, the actual samples that were cross-sectioned were not imaged in the SEM, but instead representative samples were produced using the same parameters as the samples that were cross-sectioned using the FIB mill and analyzed using the TEM.

The resulting micro/nanostructure for mounds and NC-pyramids after laser processing can be seen in Fig. 1. The SEM images shown in Fig. 1 are from representative samples produced using the same parameters as the samples sent for analysis.

TEM images of cross-sections of both mound and NC-pyramid structures, detailed in Fig. 2, reveal that both morphologies consist of a solid material for the bulk of the structure and a layer of nanoparticles coating the surface.

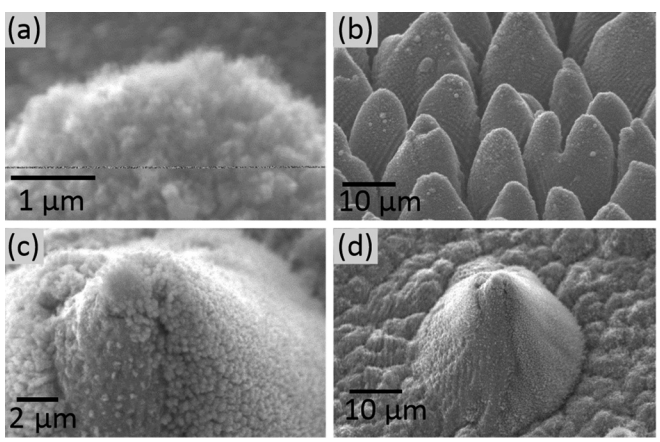

FIG. 1. SEM images of (a) and (b) mounds produced with 940 pulses/area at a fluence of 1.99 J/cm2 and (c) and (d) NC-pyramids produced using 16 820 pulses/area at 0.15 J/cm^2.

This article is copyrighted as indicated in the article. Reuse of AIP content is subject to the terms at: http://scitation.aip.org/termsconditions. Downloaded to IP: 129.93.64.70 On: Fri, 22 Aug 2014 16:36:15

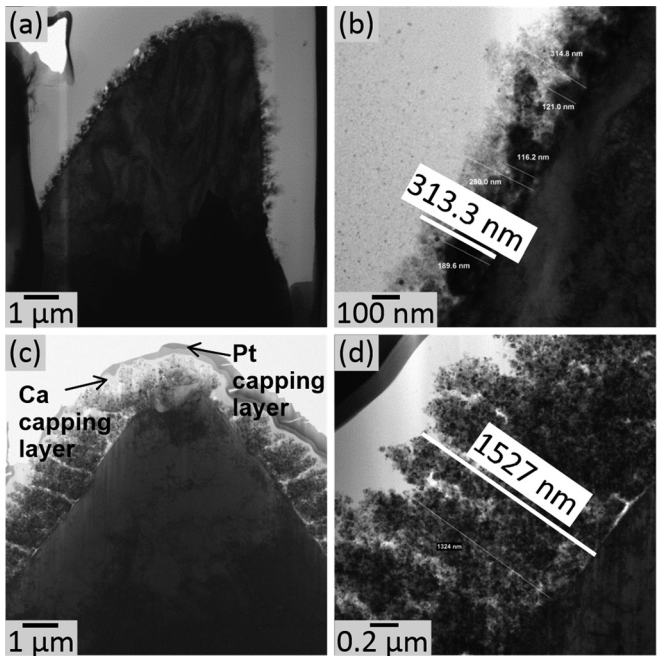

FIG. 2. TEM images of (a) and (b) a mound and (c) and (d) a NC-pyramid cross sectioned using a dual beam FIB mill.

The mounds and NC-pyramids are observed to differ in both the micrometer-scale bulk structure as well as the nanoparticle capping layer. The nanoparticle layer on the NC-pyramid is greater than 1.5 μm thick; while on the mound, it is only a few hundred nanometers thick. Upon close inspection, the nanoparticles for both samples have a large range in size from a couple hundred nanometers down to a few nanometers in diameter. It is interesting to note that a nanoparticle layer was not observed in our previous publication in which mounds were formed with a stationary beam.[18] However, nanoparticles did accumulate on regions outside the ablation crater. This dependence on rastering suggests that redeposited nanoparticles accumulate on the surface of an individual mound as regions near, but not directly over the mound, are ablated. Mounds form in a fluence range where there is significant melting and material fluid flow on the surface. Therefore, for stationary ablation (non rastering), any nanoparticles that have redeposited will melt or be ejected from the surface during subsequent ablation pulses. In contrast, NC-pyramids form in a fluence range resulting in minimal melting of the surface, and consequently nanoparticles redeposit on the NC-pyramid structures with either stationary or rastered pulses.[20,21]

Electron diffraction images of multiple locations within the bulk micrometer-scale substrate of both mounds and NC-pyramids were used to gain insight into the effect of growth mechanisms on the internal structure of the resultant surface morphologies; the corresponding TEM images are shown in Fig. 3 along with the TEM image maps that show the locations where the electron diffraction analysis were performed. This work focuses on the overall makeup of the entire mound and NC-pyramid microstructure, so the FIB mill cross sectioning was carried out in a manner to provide a broad view of the structure rather than isolating individual nanoparticles. As a result, the cross sections were not ideal for obtaining clean electron diffraction images from individual nanoparticles in the capping layer, and therefore electron diffraction images are only included for the internal structure.

TEM images show that the internal structure of the mound is characterized by numerous grains oriented at various angles, along with bending of the crystalline structure. Electron diffraction was completed at seven locations within the mound, as marked by white rectangles in Fig. 3(a). Figs. 3(b) and 3(c) are the electron diffraction patterns from locations marked in Fig. 3(a) that contain the best results. One should point out that at each location, the electron diffraction pattern is different due to the various orientations of the crystalline structure. Also, in each image, the electron diffraction pattern from multiple grains is present along with the patterns that have the indices marked. Furthermore, for most of the electron diffraction locations, there was significant overlay of multiple grains and bending of the crystalline structure that the electron diffraction patterns did not match any typical diffraction pattern for any orientation of crystalline nickel. As a result of the bending, many of the individual diffraction spots were elongated into lines similar to the spot marked in Fig. 3(f). The presence of multiple grain boundaries combined with significant strain in the crystalline structure is consistent with fluid flow and material redeposition as the dominant

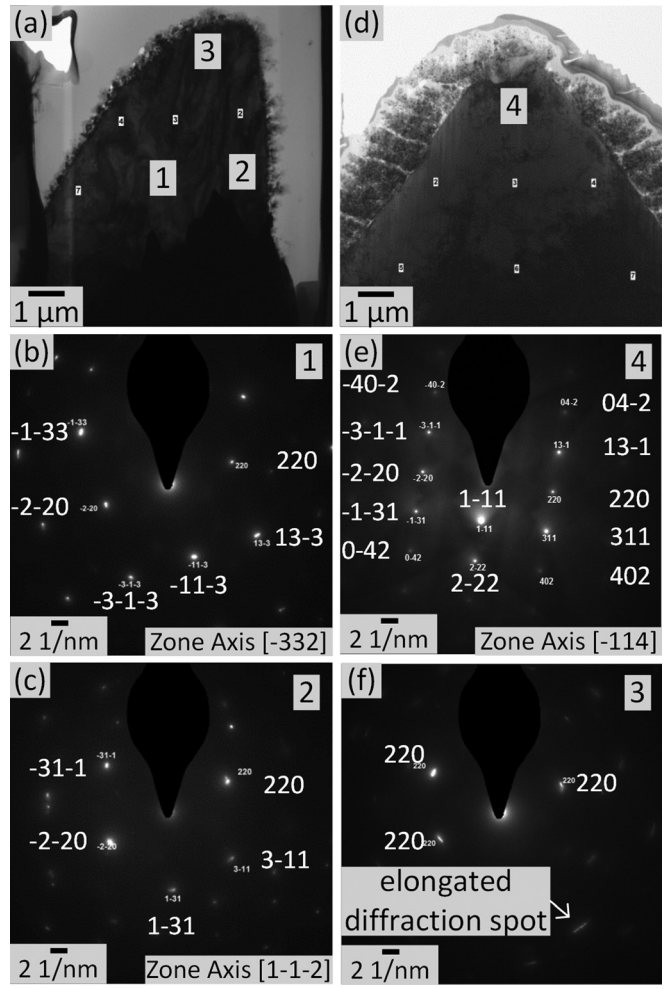

FIG. 3. (a) TEM image of a cross-sectioned (a) mound and (d) NC-pyramid with electron diffraction locations marked. (b), (c), (e), and (f) electron diffraction images from the corresponding numbered locations on the TEM images.

This article is copyrighted as indicated in the article. Reuse of AIP content is subject to the terms at: http://scitation.aip.org/termsconditions. Downloaded to IP: 129.93.64.70 On: Fri, 22 Aug 2014 16:36:15

mechanisms for the formation of mound structures over several hundred pulses.[18] It is therefore expected that the integrity of the crystalline lattice of the substrate material is directly related to the laser fluence used during FLSP and thus the degree to which the substrate was heated during the fabrication process. The visible striations (variable contrast) observable in the bulk substrate in Fig. 3(a) may be a further indication of the influence of melting during fabrication.

In the electron diffraction studies of the NC-pyramid, we observe a substantially different diffraction pattern from that of the mound. The entire NC-pyramid appears to be a single grain. Electron diffraction was completed for seven different locations in the NC-pyramid, as marked by white rectangles in Fig. 3(d). Every location that we tested produced the same diffraction pattern, which was identical to the pattern in Fig. 3(e). This consistency in crystalline structure of the NC-pyramids suggests that the growth mechanism of the NC-pyramids involves minimal laser-induced melting. Indeed, the relatively low laser fluence near the ablation threshold minimizes thermal effects during processing and agrees with the electron diffraction results. This explanation is consistent with the absence of striations in Fig. 3(d) as compared to Fig. 3(a); the contrasted regions within the NC-pyramid that are visible in Fig. 3(d) are due to variations in sample thickness from FIB milling process.

It is possible that the stark contrast between the electron diffraction analyses of the mounds and NC-pyramids was due to the original grain structure of the substrate. The specific NC-pyramid analyzed could have originated from a single grain and the ablation process left the structure unaltered. XRD analysis, not included here, indicated that the original material was not single grain, though the results did not reveal the grain sizes. However, both samples were produced on the same piece of nickel and it is unlikely that the NC-pyramid happened to form on a single large grain ($>10\,\mu$m) and the mound formed on a location with numerous nanometer-scale grains observed during the analysis. Another possibility for the NC-pyramid being composed of a single grain is that enough heat was introduced to the bulk material to anneal but not melt the structure.

For both mounds and NC-pyramids, an oxide is present throughout the nanoparticle layer, while the inner structure is pure nickel. These results were found by studying the chemical composition as a function of position within the cross-section of both the mound and NC-pyramid using scanning tunneling electron microscopy (STEM) combined with EDX analysis. Fig. 4 contains HDAAF images with locations marked where STEM/EDX analysis was completed. Table I contains the STEM/EDX results. Since EDX is only semi-quantitative, there are large error values associated with the presented atomic percentages. However, the important results demonstrated in Table I are that nickel and an oxide are present for each analyzed region in the nanoparticle layer, while the inner structure contains only nickel. The samples were laser processed in open air, and consequently it is expected that over time any portions of the surface exposed to the atmosphere would develop an oxide, regardless of the structure profile. The presence of chlorine in the analysis is not a result of laser processing, but rather is a result of the preparation process for ion beam milling. The solid, pure nickel core supports the theory of fluid flow of the surface melt and preferential ablation processes for the formation of each of these structures.

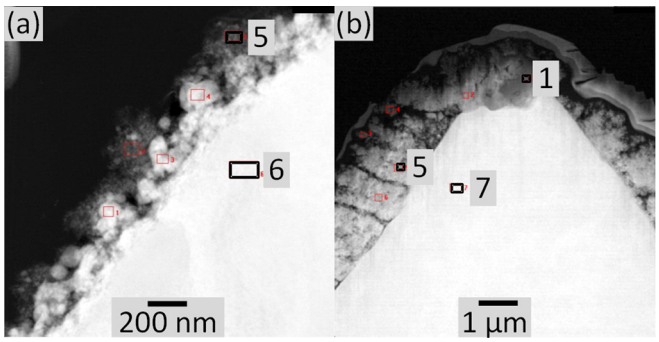

FIG. 4. High-angle annular dark-field TEM images of (a) a mound and (b) a pyramid with the regions marked where EDX was completed.

Notice in Table I that the tip of the NC-pyramid contains a high concentration of aluminum, oxygen, and some titanium. This impurity region is likely a result of the polishing process completed by the material vendor, which utilized alumina powder. It is expected that this impurity has a higher ablation threshold than the pure nickel bulk material, which would result in the formation of the precursor cone as discussed in our previous publication.[20,21] This polishing-induced impurity is expected to be one of many potential sources for precursor cone formation. Through other studies not described here, similar precursor sites have been observed on unpolished surfaces as well as within the bulk of the material where any surface effects do not play a role. Future studies will further clarify the sources of precursor cone formation.

This work documents the structural and chemical composition of two unique structures: mounds and NC-pyramids formed by FLSP. Both morphologies are shown to have a solid core made of the original material (nickel), overlaid with nickel oxide nanoparticles. The NC-pyramid structures are made of a single grain while the mound structures contain many grains oriented at various angles along with bending of the crystalline structure. These results demonstrate the impact of the laser fluence on the integrity of the underlying crystalline structure as well as on the surface profile generated during multishot laser ablation processes. For this reason, modifications of the internal structure of the target material cannot be neglected when using such laser parameters to tailor the surface morphology. Additionally, attempts to model the development of multiscale structures through femtosecond laser illumination must account for the impact of laser fluence on the physics of the light-matter interaction.

TABLE I. EDX results giving the atomic percentages for each area marked in Fig. 4.

Sample		Ni (atom %)	O (atom %)	Cl (atom %)	Al (atom %)	Ti (atom %)
Mound	area 5	47.09	46.31	6.59	…	…
	area 6	100.00	…	…	…	…
NC-pyramid	area 1	0.48	60.11	…	37.63	1.76
	area 5	53.58	46.41	…	…	…
	area 7	100.00	…	…	…	…

This article is copyrighted as indicated in the article. Reuse of AIP content is subject to the terms at: http://scitation.aip.org/termsconditions. Downloaded to IP: 129.93.64.70 On: Fri, 22 Aug 2014 16:36:15

We would like to thank Evans Analytical Group (EAG) for providing the cross-sectioning and TEM analysis of the samples. We would also like to thank Dr. Xingzhong Li, in the NCMN at UNL for assistance with interpreting the crystalline structure from electron diffraction analyses. This work has been supported by a Multi-University Research Initiative (MURI) No. W911NF-06-1-0446, Grant Assistance in Areas of National Need (GAANN) No. P200A070344, and a grant through the Nebraska Center for Energy Sciences Research (NCESR) with funds provided by Nebraska Public Power District (NPPD) to the University of Nebraska-Lincoln (UNL) No. 4200000844.

[1]M.-J. Sher, M. T. Winkler, and E. Mazur, MRS Bull. **36**, 439 (2011).
[2]C. H. Crouch, J. E. Carey III, M. Shen, E. Mazur, and F. Y. Genin, Appl. Phys. A **79**, 1635 (2004).
[3]R. Younkin, J. E. Carey III, E. Mazur, J. A. Levinson, and C. M. Friend, J. Appl. Phys. **93**, 2626 (2003).
[4]C. Wu, C. H. Crouch, L. Zhao, J. E. Carey III, R. Younkin, J. A. Levinson, E. Mazur, R. M. Farrell, P. Gothoskar, and A. Karger, Appl. Phys. Lett. **78**, 1850 (2001).
[5]A. Y. Vorobyev and C. Guo, Appl. Phys. Lett. **92**, 041914 (2008).
[6]A. Y. Vorobyev and C. Guo, Opt. Express **18**, 6455 (2010).
[7]A. Y. Vorobyev and C. Guo, J. Appl. Phys. **108**, 123512 (2010).
[8]B. Wu, M. Zhou, J. Li, X. Ye, G. Li, and L. Cai, Appl. Surf. Sci. **256**, 61 (2009).
[9]T. Baldacchini, J. E. Carey, M. Zhou, and E. Mazur, Langmuir **22**, 4917 (2006).
[10]B. K. Nayak and M. C. Gupta, Opt. Lasers Eng. **48**, 940 (2010).
[11]N. G. Semaltianos, W. Perrie, P. French, M. Sharp, G. Dearden, S. Logothetidis, and K. G. Watkins, Appl. Phys. A **94**, 999 (2009).
[12]T. Y. Hwang and C. Guo, J. Appl. Phys. **111**, 083518 (2012).
[13]T. H. Her, R. J. Finlay, C. Wu, and E. Mazur, Appl. Phys. A **70**, 383 (2000).
[14]M. Tsukamoto, T. Kayahara, H. Nakano, M. Hashida, M. Katto, M. Fujita, M. Tanaka, and N. Abe, J. Phys.: Conf. Ser. **59**, 666 (2007).
[15]M. A. Sheehy, L. Winston, J. E. Carey, C. M. Friend, and E. Mazur, Chem. Mater. **17**, 3582 (2005).
[16]B. K. Nayak, M. C. Gupta, and K. W. Kolasinski, Appl. Surf. Sci. **253**, 6580 (2007).
[17]B. K. Nayak, M. C. Gupta, and K. W. Kolasinski, Appl. Phys. A **90**, 399 (2008).
[18]C. A. Zuhlke, T. P. Anderson, and D. R. Alexander, Opt. Express **21**, 8460 (2013).
[19]S. Amoruso, R. Bruzzese, X. Wang, N. N. Nedialkov, and P. A. Atanasov, J. Phys. D: Appl. Phys. **40**, 331 (2007).
[20]C. A. Zuhlke, *Control and Understanding of the Formation of Micro/Nanostructured Metal Surfaces Using Femtosecond Laser Pulses* (University of Nebraska, 2012).
[21]C. A. Zuhlke, T. P. Anderson, and D. R. Alexander, Appl. Surf. Sci. **283**, 648–653 (2013).

This article is copyrighted as indicated in the article. Reuse of AIP content is subject to the terms at: http://scitation.aip.org/termsconditions. Downloaded to IP: 129.93.64.70 On: Fri, 22 Aug 2014 16:36:15